Journal of Biomechanics 83 (2019) 157–164

Contents lists available at ScienceDirect

Journal of Biomechanics

journal homepage: www.elsevier.com/locate/jbiomech
www.JBiomech.com

A manipulability analysis of human walking

Behnam Miripour Fard

Faculty of Mechanical Engineering, University of Guilan, Rasht, Iran

ARTICLE INFO

Article history:
Accepted 23 November 2018

Keywords:
Manipulability
Bipedal walking
Swing phase
Strategy selection
Kinematics

ABSTRACT

From the literature of biomechanics, it is now clear that humans use elevating, lowering and delayed-lowering strategies in order to maintain stability during perturbed walking. The main purpose of this study is to provide insights into the role of manipulability in selection of these strategies. A 37 degrees of freedom (DoFs) model of the human body is developed to evaluate the manipulability indices during walking. The model is considered as a tree-like structure and its forward kinematics equations and the Jacobian are derived based on the Denavit-Hartenberg (DH) convention. A hybrid genetic algorithm (HGA) is then employed to map the experimental kinematics of a human to the model. The kinematic and dynamic manipulability indices of the swing phase of walking are evaluated concentrating on early, mid and late swing phases. The results indicate that the manipulability indices can characterize well the selection of elevating, lowering and delayed-lowering strategies at different stages of the swing phase. The results kinematically describe the reason of selecting delayed-lowering strategy at mid-swing phase that was not obvious in previous studies. Moreover, the results show that at mid-swing phase of walking the kinematic maneuverability is lower than that of the early and late swing phases.

1. Introduction

In the field of biomechanics and humanoid robotics, researchers have previously explored many measures (e.g. jerk, metabolic energy, stability and etc.) to find out the formation of human movements during walking (Xiang et al., 2010). However, the evaluation of manipulability indices during walking has not been extensively studied. In the case of serial manipulators, the manipulability is a quantitative measure showing the capacity to change the end effector's position and velocity (Spong et al., 2006). In the other words, the manipulability is the measure of dexterity. When the manipulator is in a singular configuration, the manipulability approaches to zero. The concept of kinematic Manipulability for robotic manipulators was first introduced and discussed in (Yoshikawa, 1985b). A dynamic manipulability measure for robot arms, which takes the dynamics into consideration, has also been introduced in (Yoshikawa, 1985a).

Human body has a tree-like structure consisting of a number of serial branches such as legs, arms, and head, all connected to the same trunk. The end of each of these branches can be considered as the end effector of a serial manipulator. Given a particular posture of the trunk, manipulability allows to assess the set of velocities that can be achieved by the tip of the swing leg. The manipulability measures how easy or difficult it is for a human to move his/her swing limb in a given direction. It is a velocity-based measure that can determine potential foot placement possibilities and consequently influence the stability and maneuverability of walking (Pratt and Tedrake, 2006). Foot placement is one of the most important factors for biped stability (Castano et al., 2016). It is important to understand how the central nervous system (CNS) coordinates the redundant DOFs of the body and selects particular strategies or foot positions during walking.

To the best of current author knowledge, the evaluation of manipulability index during normal and perturbed walking has never been the subject of a study on human. A vast body of previous studies has focused on the manipulability and coordination of the upper DOFs for hand movements and grasping tasks. For example, Jacquier-Bret et al. (2013) analyzed the coordination of upper-limb joints using manipulability indices (Jacquier-Bret et al., 2013). Endo (2015) has evaluated manipulability during smartphone thumb-based touch operations and concluded that this index is a useful measure for quantitatively evaluation of human hand operations (Endo, 2015). Vahrenkamp et al. (2012) used an extended manipulability measure to investigate grasping selection of a humanoid robot (Vahrenkamp et al., 2012). The measure is based on the consideration of joint and workspace limitations. Kobayashi et al. (2013) have proposed the dynamic reconfiguration manipulability (DRM) index for humanoid robots (Kobayashi et al., 2013). Given a prior end-effector task, DRM indicates a shape-changeability of each intermediate link (Minami et al., 2010).

E-mail address: bmf@guilan.ac.ir

https://doi.org/10.1016/j.jbiomech.2018.11.038
0021-9290/

Kobayashi et al. (2013) implemented DRM index for lifting task and for walking shape of crouching down and stretching humanoid's leg (Kobayashi et al., 2013). Their simulation model had 18 degrees of freedom and they did not use experimental data for confirmation of results. Jacquier-Bret et al. (2012) have evaluated upper limb movements during a reach to grasp movement using manipulability index (Jacquier-Bret et al., 2012). They have concluded that the volume of manipulability ellipsoid reflects well the ability of upper extremity to generate speed at the wrist.

Due to the redundancy of human body, there are many strategies that humans can adopt to maintain stability during walking or after a perturbation. From the experimental studies on human walking, it is now clear that humans adopt three main strategies to prevent falling (Eng et al., 1994; Eng et al., 1997):

- Elevating strategy which consists of elevation of the swing leg. In this strategy, the step is lengthened.
- Lowering strategy consists of bringing the foot to the ground as quickly as possible. The step lengths and time are reduced,
- Delayed-lowering strategy could be understood as a failed elevating strategy in which the subject first tries an elevating strategy and then switches to a lowering one.

Elevating and lowering strategies are adopted in response to early and late swing perturbations, respectively (Eng et al., 1994; Potocanac et al., 2014; Wang et al., 2012). Around mid-swing phase of walking, the strategy selection is not mechanically obvious (Potocanac et al., 2016; Roos et al., 2009).

The main purpose of current study is to characterize strategy selection during walking, using the manipulability index.

2. Material and methods

2.1. Multibody modeling and forward kinematics

The model of this study is depicted in Fig. 1a. The human body is modeled using a series of rigid links connected by revolute joints. With consideration of 6 global DOFs, the total DOFs of the model of this study is 37. The model has a tree-like structure. Each of the fourteen segments of the model can be considered as the base or the root. In the current study, the stance foot is chosen as the root. Considering right foot as the support, there are three branches for the model: the left leg, the right arm and the left arm (Fig. 1b). It is obvious that in this tree-structured kinematic chain, some joints do not influence the motion of some chains.

The tree-structured model of the current study consists of three serial sub-structures. Fig. 2 shows the topology of the model.

For each of the serial sub-structures, the serial segment conventions are used without change. The DH notation (Denavit and Hartenberg, 1955) is used for geometric description of the human model. Based on (Spong et al., 2006), the transformation matrix is equal to

$$ {}^{j-1}\boldsymbol{T}_j = \begin{bmatrix} \cos q_j & -\sin q_j \cos \alpha_j & \sin q_j \sin \alpha_j & a_j \cos q_j \\ \sin q_j & \cos \alpha_j \cos q_j & -\cos q_j \sin \alpha_j & a_j \sin q_j \\ 0 & \sin \alpha_j & \cos \alpha_j & d_j \\ 0 & 0 & 0 & 1 \end{bmatrix} \quad (1) $$

where the four quantities q_j, a_j, d_j and α_j are parameters associated with link j and joint j ($j = 1, 2, \ldots$ m = number of DoFs). α_j is the angle between z_{j-1} and z_j measured about x_j (see Fig. 1a). a_j and

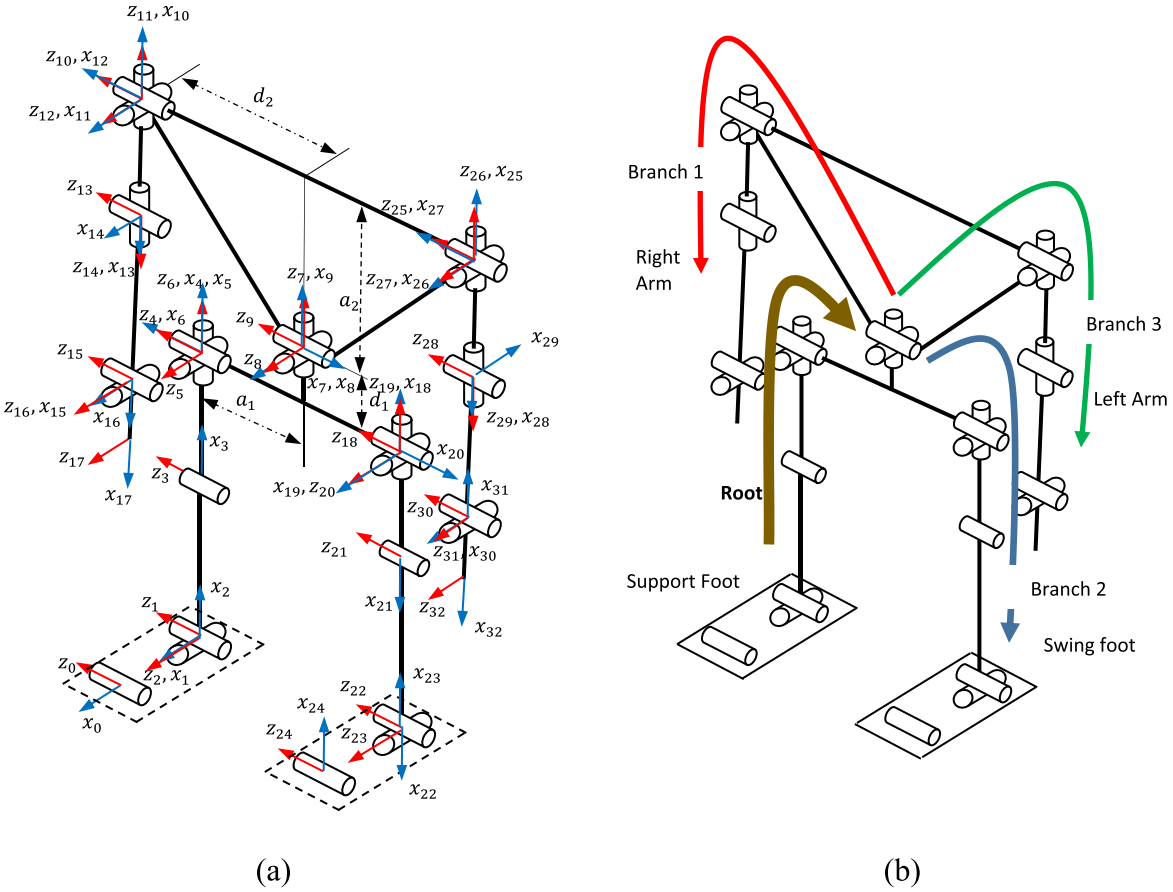

Fig. 1. (a) Model of the current study (b) root and branches of the model.

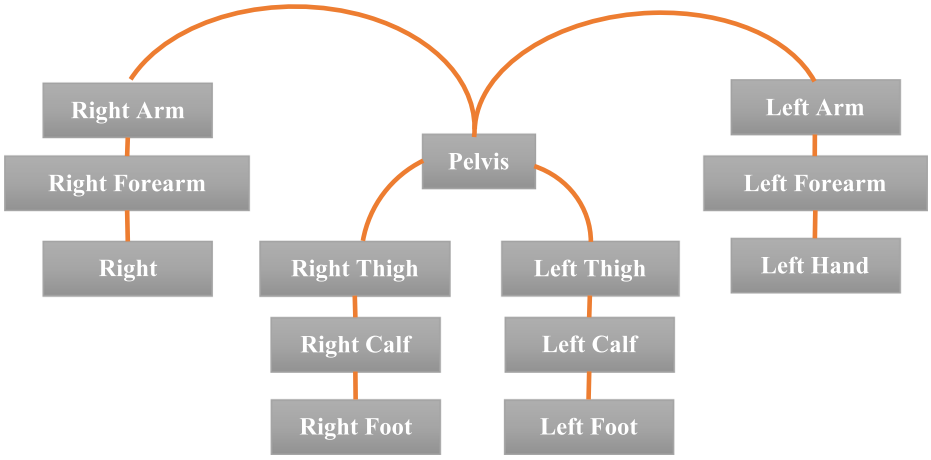

Fig. 2. Topology of the model.

d_j are the constant anthropometric parameters that are obtained using the distances between the real markers on the human subject. The geometric model of the human will be obtained by the successive multiplication of the transformation matrices.

$$^{0}\mathbf{T_m}=^{0}\mathbf{T_1}^{0}\mathbf{T_2}\ldots^{\mathbf{m-1}}\mathbf{T_m} \tag{2}$$

2.2. Jacobian matrix

The Jacobean matrix is only calculated for the swing phase of walking. The model has three serial sub-structures with three end-effectors. So, the body velocity in the right hand of the Eq. (3) is a $6N \times 1$ vector ($N = 3$), and the Jacobian matrix is a $6N \times 31$ matrix

$$\begin{pmatrix} \xi_1 \\ \xi_2 \\ \xi_3 \end{pmatrix} = \begin{pmatrix} \boldsymbol{J}_1^1 & \boldsymbol{J}_1^2 & \boldsymbol{J}_1^3 \\ \boldsymbol{J}_2^1 & \boldsymbol{J}_2^2 & \boldsymbol{J}_2^3 \\ \boldsymbol{J}_3^1 & \boldsymbol{J}_3^2 & \boldsymbol{J}_3^3 \end{pmatrix} \begin{pmatrix} \dot{q}_1 \\ \vdots \\ \dot{q}_{31} \end{pmatrix} \tag{3}$$

Formally, the above relationship can be expressed as

$$\xi = \boldsymbol{J}\dot{\boldsymbol{q}} \tag{4}$$

It should be noted that the Jacobian matrix has many zero elements on the places where some joints do not influence the motion of some end-effectors.

2.3. Manipulability measures

From the kinematics aspect, for a given configuration of a manipulator, ellipsoid of manipulability is drawn considering unit norm joint velocities as the input. Two following indices are usually derived from the kinematic manipulability ellipsoid:

(a) The first index which is proportional to the volume of the ellipsoid is defined as

$$w_1 = \sqrt{\det(\boldsymbol{J}\boldsymbol{J}^T)} = s_1 s_2 \cdots s_m \tag{5}$$

where s_i is the singular value of the Jacobian ($\boldsymbol{J}$) and det is the determinant of the ($\boldsymbol{J}\boldsymbol{J}^T$). m is the number of DoFs. This index represents the global end-effector capacity for velocity generation. For a 6 DOF manipulator, when the Jacobian loses rank, w_1 equals zero meaning that the manipulator is in a singular configuration. For a redundant manipulator, when the Jacobian loses rank, the manipulability ellipsoid loses dimensions to either an ellipse or a line. The higher values of w_1 imply that the manipulator is in the posture that gives it the best ability to move.

(b) The second index is called condition number (Klein and Blaho, 1987). The condition number is defined as

$$w_2 = \frac{s_l}{s_s} \tag{6}$$

in which s_s and s_l are the smallest and largest singular values of the Jacobian, respectively. This index represents the distribution of the end-effector capacity of velocity generation along each direction of the Cartesian task space. When $w_2 = 1$, the ellipsoid approaches a spherical shape, indicates that the capability of tangential velocity generation is similar in every direction (isotropic configuration).

The aforementioned manipulability indices are based on the kinematics and the dynamics are ignored. Analysis of dynamic manipulability has also been performed in the current work. A dynamic manipulability measure has been defined which takes into consideration the dynamics of motion. This measure specifies the ability to perform end-effector accelerations in a given posture with the joint torques constrained to belong to a unit sphere (Yoshikawa, 1990). Assume that the dynamics of the model is presented by Eq. (7) as follows

$$\boldsymbol{M}(\boldsymbol{q})\ddot{\boldsymbol{q}} + \boldsymbol{C}(\boldsymbol{q}, \dot{\boldsymbol{q}}) + \boldsymbol{G}(\boldsymbol{q}) = \boldsymbol{\tau} \tag{7}$$

where $\mathbf{q} \in \mathbb{R}^{31}$ is the vector of generalized joint angles (depicted in Fig. 1a), $\mathbf{M}(\mathbf{q}) \in \mathbb{R}^{31\times31}$ is the mass-inertia matrix, $\mathbf{C}(\mathbf{q}, \dot{\mathbf{q}}) \in \mathbb{R}^{31}$ contains the centrifugal and Coriolis forces terms, $\mathbf{G}(\mathbf{q}) \in \mathbb{R}^{31}$ is the vector of gravitational forces, $\tau \in \mathbb{R}^{31}$ is the vector of joint torques. The dynamics equations of the model were derived using the Euler-Lagrange formulation (Spong et al., 2006). Based on Yoshikawa (1990), the Jacobian matrix and the mass-inertia matrix are used to obtain the dynamic manipulability measure as follows

$$w_d = \sqrt{\det(\boldsymbol{J}(\boldsymbol{M}^T\boldsymbol{M})^{-1}\boldsymbol{J}^T)} \tag{8}$$

The detailed mass/inertia parameters as a fraction of total height and weight were obtained according to anthropometric tables (Winter, 2009).

2.4. Kinematic mapping

In this section, mapping of human kinematics on the model of Fig. 1a is presented. This is accomplished using an inverse kinematic method. In this method, the positions of the real markers

on the human body are given and the joint angles of the model should be obtained (Huang et al., 2010). To find the best match between the model and experimental kinematics, an optimization problem is solved in each time step of motion. First, virtual markers are placed on the model that correspond to the position of the physical markers on the human subject. Then, the distances between the virtual and the corresponding experimental marker positions are minimized. The cost function is expressed as

$$\text{Cost} = \min_{\mathbf{q}} \sum_{i=1}^{n} w_i \| x_i^{\text{exp}} - x_i^{v}(\mathbf{q})^2 \| \tag{9}$$

in which $\mathbf{q}$ is a vector composed of joint angles, x_i^{exp} is the position of experimental marker i, $x_i^{v}(q)$ is the position of the corresponding virtual marker i. n is the number of markers. w_i is the weight associated with marker i. Value of the weight of each marker specifies the importance of that marker's error term in the optimization

Table 1
Value of the weights ($\boldsymbol{w_i}$) used in the optimization cost.

Marker name	Weight	Marker name	Weight	Marker name	Weight
Right toe	1	Right ankle	10	Right knee	10
Left toe	1	Left ankle	10	Left knee	10
Right hip	10	Right wrist	5	Right shoulder	10
Left hip	10	Left wrist	5	Left shoulder	10
Right elbow	20	Right hand	30	pelvis	10
Left elbow	20	Left hand	30		

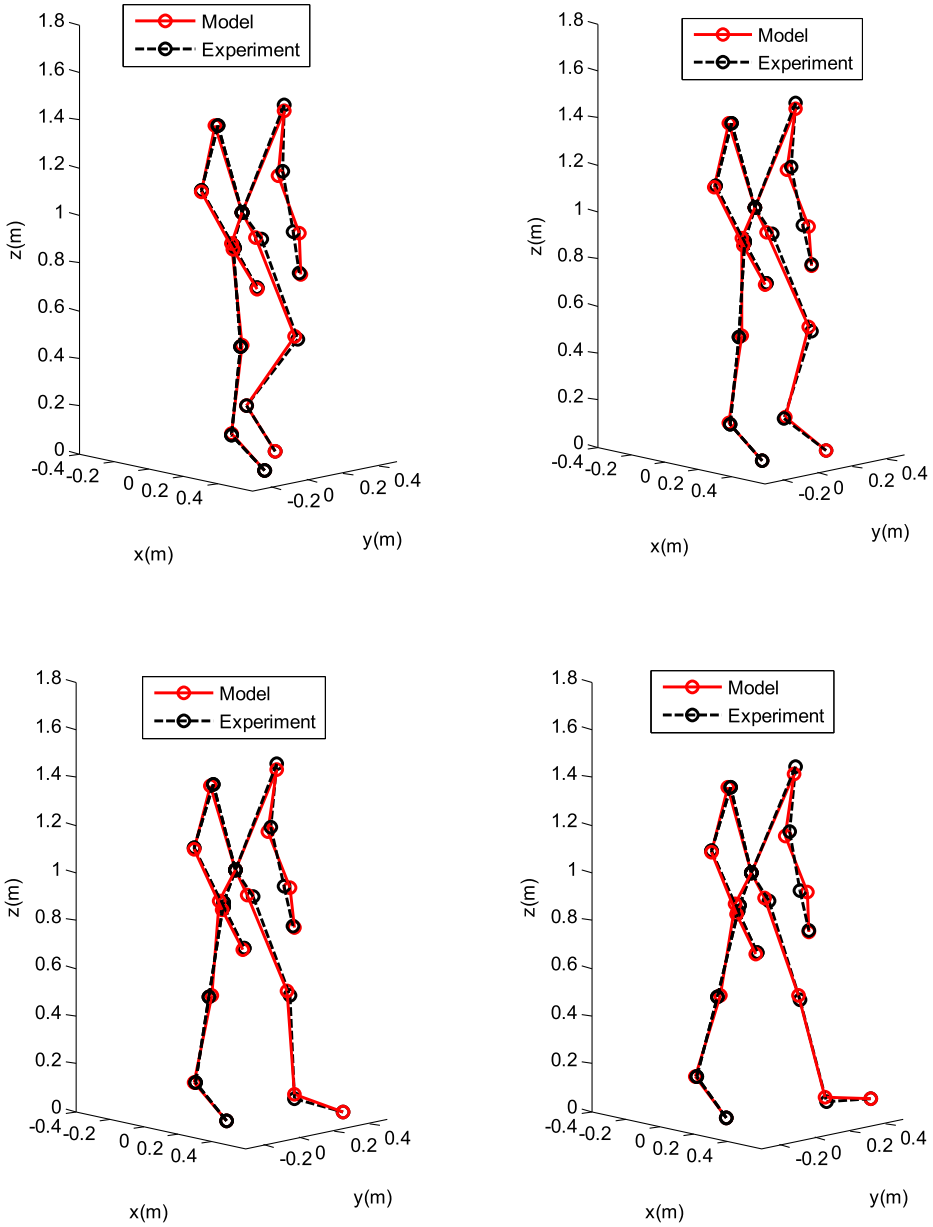

Fig. 3. Comparison of the four selected snapshots of walking between model and experiment.

problem. The joint angles (**q**) are the design variables of the optimization in each frame of motion. The cost function is subject to the constraints on physiological limitation of joint angles. The lower and upper bounds on the design variables (in radians) are considered as follows, respectively:

lb = [−60, 60, 0, 0, −30, 40, 160, −30, 70, −70, −130, −120, −10, 90, −50, −110, −30, 120, 60, −120, −90, −200, 0, 150, −110, 50, −90, 150, 50, 150] * π/180;
ub = [60, 150, 10, 60, 90, 120, 210, 30, 120, 20, 30, −60, 120, 180, 50, −70, 30, −30, 120, −60, 0, −160, 10, 0, −70, 180, 60, 210, 130, 210] * π/180;

In each frame of motion, the above mentioned optimization problem is solved using a commercial software package (MATLAB release 2014a, The MathWorks, Inc., Natick, MA, USA) and the output which is a vector of joint angles (**q**) is saved for future uses. In the current work, a hybrid genetic algorithm (HGA) which combines both deterministic and stochastic routines (Gen et al., 2017) was used to solve the problem.

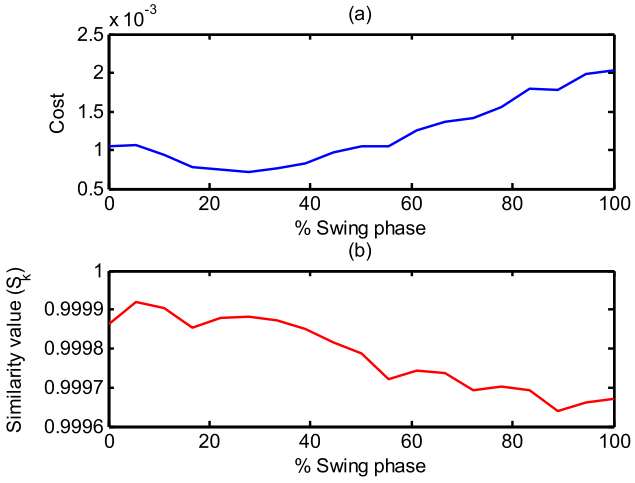

Fig. 4. (a) The cost of optimization problem. Unit of the parameters of the cost function is the meter. (b) Similarity value of mapping experimental data to the simulation model.

To evaluate the similarity between the results of solving the optimization problem and kinematics of human subject, a function from the work of Zhao et al. (2004) is used in the current work. Given the step time k, similarity function is expressed as

$$S_k = \frac{1}{1 + \sum_{i=1}^{n} \left(\frac{o_{mi} - o_{si}}{o_{mi}^{\max} - o_{mi}^{\min}} \right)^2} \tag{10}$$

where o_{mi} denotes the position of the marker i of the model (virtual marker) with respect to the reference coordinate system. The values of o_{mi} is calculated by inserting the optimal values of the joint angles in the forward kinematic equations using MATLAB. o_{si} represents the corresponding position of the marker i on the human subject (real marker) with respect to the same reference coordinate system. $o_{mi}^{\max}$ and $o_{mi}^{\min}$ are the upper and lower bounds of the range of motion of the marker i-th, respectively. n is the number of markers. It should be noted that S_k is always $0 < S_k \leqslant 1$. If $S_k = 1$ the similarity would be maximal.

The experimental motion capture data used in this study were obtained from the work (Bruijn et al., 2010). In the above mentioned work, eleven young healthy male persons (age 27.7 ± 3.3 years, mass 75.5 ± 9.0 kg, height 1.80 ± 0.06 m; means ± s.d.) walked on the treadmill and the kinematic data of reflective markers were sampled at 50 Hz. All the persons signed an informed consent form before starting trials. The protocol has been approved by the ethical committee of the Faculty of Human Movement Sciences of VU University, Amsterdam. 3D optoelectronic system (Optotrak® Northern Digital Inc., Waterloo, ON, Canada) has been used for kinematic data collection of reflective markers. In the current work, the data of the eleven subjects are used. The subjects walked at speed 1.68 ms^{-1} for 5 min (one trial per person) without perturbation (steady-state walking).

3. Results and discussion

First, the results of similarity are presented. Value of the weights of the markers (w_i) in Eq. (9) is presented in Table 1. Fig. 3 presents the snapshots of four selected frames of motion. As can be seen, there are good accordance between the kinematics of human and corresponding model.

For quantitative evaluation, the similarity value (Eq. (10)) and the cost of optimization problem (Eq. (9)) are depicted in Fig. 4.

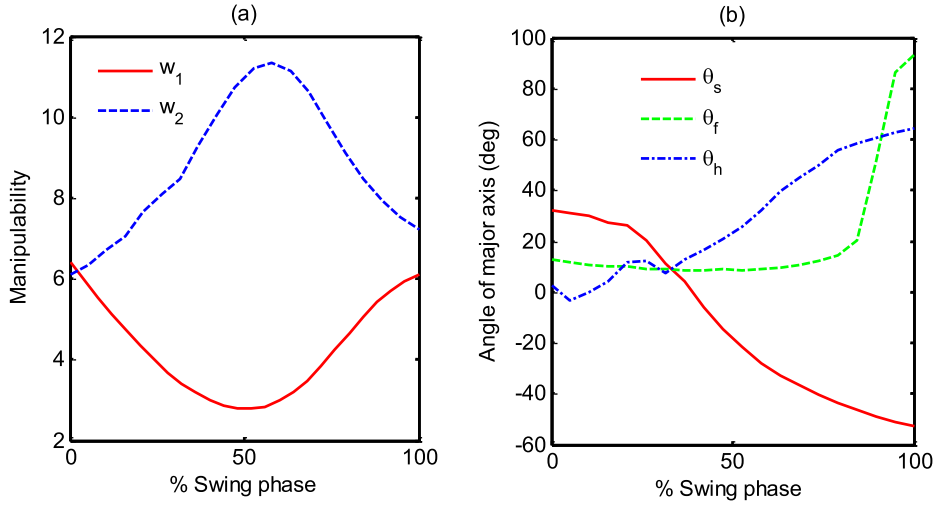

Fig. 5. (a) The mean of the kinematic manipulability and condition number of the tip of the swing foot for eleven subjects (b) angles formed by the major axis of the projection of the kinematic manipulability ellipsoid with the positive directions of the reference coordinate system. θ_s stands for sagittal plane angle (rotates CW during swing phase, see Fig. 6b), θ_f stands for frontal plane angle (rotates CCW, see Fig. 6c) and θ_h stands for horizontal plane angle (rotates CCW, see Fig. 6d).

The results of similarity evaluation are relatively fair. These results are reasonable because the model is redundant and a global optimization algorithm (HGA) was used to solve the problem.

Fig. 5a shows the evolution of the mean of the manipulability index and condition number of the tipping point of the swing foot during walking. It is seen that during the mid-swing phase of walking the kinematic manipulability is lower than that of the early and late swing phases, contrary to what happens with condition number. The results indicate a greater range of possible motions at the early and late swing phases of walking. Variation of the angle of the major axis of the projection of the manipulability ellipsoid onto the sagittal, frontal and horizontal planes have been depicted in Fig. 5b. For qualitative presentation of the results of Fig. 5, the 3D ellipsoids of manipulability are presented in Fig. 6a. In addition, Fig. 6b–d show the sagittal, frontal and horizontal projection of the manipulability ellipsoid during swing phase of walking, respectively.

It should be mentioned that the shape and the orientation of the manipulability ellipsoid are affected by the human posture. This helps to establish a standard metric such that a variety of postures can be compared. Given a posture of the human and based on the definition of the manipulability ellipsoid, the swing foot has better capacity of motion in the direction of the major axis. The direction of the minor axis represents the direction with worse capacity of developing speed. Regulating the velocity of the swing limbs is the most challenging subtask for human or human-like bipedal walking (e.g. (Pratt and Tedrake, 2006)). Shape of the manipulability ellipsoids can predict the opportunity for the human to place its swing leg in such a way that it can continue walking without falling down. As a result, it can affect the selection of strategy to regain stability after being perturbed during walking. From Figs. 5 and 6, the ability to generate velocities in different directions is seen. During the early swing phase, the ability to generate velocity in +x, +z and −y directions are higher than that of the mid and late swing phases. Contrary to this, during the late swing phase, the capacity for velocity generation in +x, −z and +y is high.

The manipulability analysis of current study justifies the selection of human-observed strategies. The comparison of the manipulability ellipsoids in Fig. 6 shows that the capacity of velocity generation in +x and +z directions (+x is the direction of walking) during the early-swing phase is more than that of mid-swing and late-swing phases (Fig. 6b). So, the selection of elevating strategy

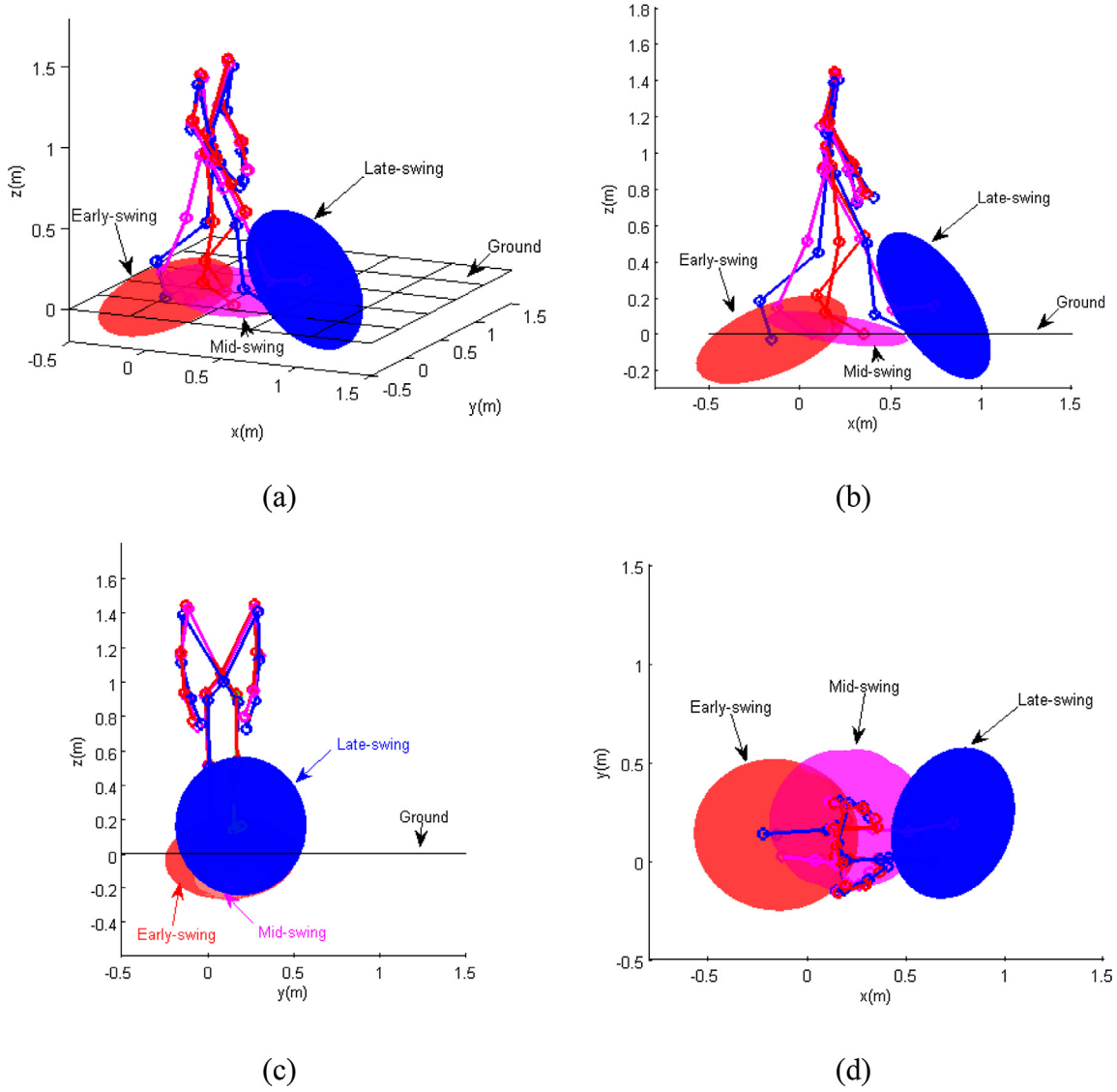

Fig. 6. Scaled down manipulability ellipsoids at early, mid and late-swing phase of walking. (a) 3D view (b) sagittal view (c) frontal view (d) horizontal view. The left foot is in the swing phase.

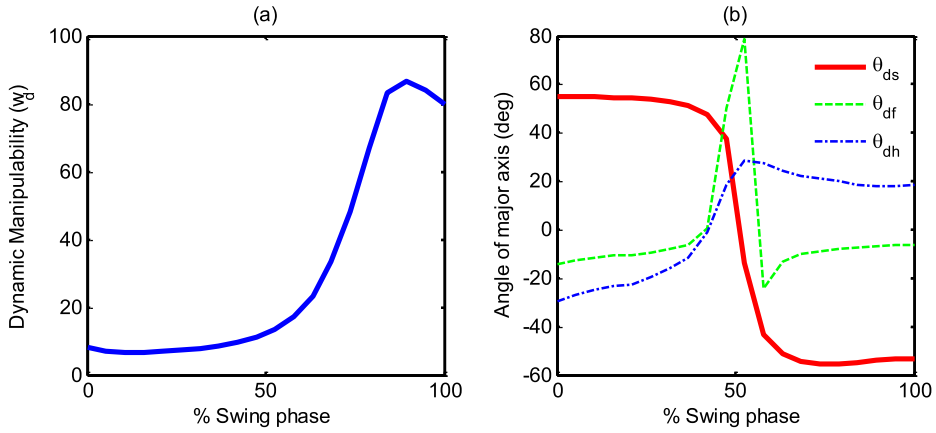

Fig. 7. The mean of the dynamic manipulability measure during swing phase (b) angles formed by the major axis of the projection of the dynamic manipulability ellipsoid with the positive directions of the reference coordinate system. θ_{ds} stands for sagittal plane angle (rotates CW during swing phase), θ_{df} stands for frontal plane angle and θ_{dh} stands for horizontal plane angle (rotates CCW).

at early-swing phase is feasible. Also, the capacity of velocity generation in -z direction at the late swing phase is more than that of the early swing phase. Consequently, the selection of lowering strategy at the late-swing phase is more feasible. At mid-swing phase, regarding the shape of manipulability ellipsoid, the subject first tries an elevating strategy (similar to that of early swing phase), but, when goes ahead, the shape of manipulability changes in a way that induces adaptation of the lowering strategy. So, the so-called delayed-lowering strategy is observed. It should be noted that in the Fig. 6 the center of the ellipsoid for early-swing phase (which is the position of the tip of the swing foot) is located in the back of the center of the mid-swing and late-swing ellipsoids.

The evolution of the mean of the dynamic manipulability index of the swing foot during walking has been illustrated in Fig. 7a. Variation of the angle of the major axis of the projection of the dynamic manipulability ellipsoid in the sagittal, frontal and horizontal planes have been depicted in Fig. 7b. At the mid swing phase there are sharp changes in the direction of the dynamic manipulability ellipses. As can be seen from the Fig. 7, the dynamic manipulability measure significantly increases during the late swing phase. This may be judged to be a rather good situation for the human during the late swing phase. It implies that there is a wide range of realizable acceleration for the swing foot under certain constraint on the magnitude of the joint driving torques.

Considering both of the kinematic and dynamic measures, the manipulability of the late swing phase is in the better condition comparing with that of the early and mid-swing phases. The direction of dynamic manipulability ellipses (especially in the sagittal and horizontal plane) also justifies the human observed strategies as discussed earlier in the case of kinematic manipulability.

To summarize, the results of kinematic and dynamic manipulability evaluation indicate that the mid swing phase is the turning point of the almost all the manipulability curves. This justifies and characterizes the change in the strategy selection before and after the mid swing phase of walking.

4. Conclusions

In this paper, an evaluation of the manipulability of swing phase of walking was presented. The results showed that the manipulability indices can characterize the selection of elevating, lowering and delayed-lowering strategies during different stages of swing phase. The results also represent that the kinematic manipulability at mid-swing phase is less than that of the early and the late swing phases. So, the ability to generate velocity in all directions at mid-swing phase is limited. Therefore, this phase of walking needs more attention in disturbance rejection. The shape of manipulability ellipsoid at mid-swing phase of walking describes the reason for selecting the delayed-lowering strategy. This was not mechanically obvious in previous studies (Potocanac et al., 2016; Roos et al., 2009). The turning point of the manipulability happens at the mid swing phase and this can be the starting point of the strategy changes. Computing and monitoring the manipulability indices of humans/humanoid robots can be useful for several purposes, e.g. it can be used for monitoring the current state of the humans/robots to support decision processes such as strategy selection after a perturbation. These indices also can be useful if considered as a criterion in path and step planning of human assistive devices or humanoids to create robots having human levels of competence in acting.

Acknowledgement

The author expresses thanks to Dr. S.M. Bruijn for his help in obtaining the experimental data used in the present work.

Conflicts of interest statement

The authors have NO conflict of interest and affiliations with or involvement in any organization or entity with any financial interest (such as honoraria; educational grants; participation in speakers' bureaus; membership, employment, consultancies, stock ownership, or other equity interest; and expert testimony or patent-licensing arrangements), or non-financial interest (such as personal or professional relationships, affiliations, knowledge or beliefs) in the subject matter or materials discussed in this manuscript.

References

Bruijn, S.M., Meijer, O.G., Beek, P.J., van Dieën, J.H., 2010. The effects of arm swing on human gait stability. J. Exp. Biol. 213, 3945–3952.
Castano, J.A., Li, Z., Zhou, C., Tsagarakis, N., Caldwell, D., 2016. Dynamic and reactive walking for humanoid robots based on foot placement control. Int. J. Humanoid Rob. 13, 1550041.
Denavit, J., Hartenberg, R.S., 1955. A kinematic notation for lower-pair mechanisms based on matrices. Trans. ASME J. Appl. Mech. 23, 215–221.
Endo, H., 2015. Application of robotic manipulability indices to evaluate thumb performance during smartphone touch operations. Ergonomics 58, 736–747.
Eng, J.J., Winter, D.A., Patla, A.E., 1994. Strategies for recovery from a trip in early and late swing during human walking. Exp. Brain Res. 102, 339–349.
Eng, J.J., Winter, D.A., Patla, A.E., 1997. Intralimb dynamics simplify reactive control strategies during locomotion. J. Biomech. 30, 581–588.

Gen, M., Zhang, W., Lin, L., Yun, Y., 2017. Recent advances in hybrid evolutionary algorithms for multiobjective manufacturing scheduling. Comput. Ind. Eng. 112, 616–633.
Huang, Q., Yu, Z., Zhang, W., Xu, W., Chen, X., 2010. Design and similarity evaluation on humanoid motion based on human motion capture. Robotica 28, 737–745.
Jacquier-Bret, J., Gorce, P., Rezzoug, N., 2012. The manipulability: a new index for quantifying movement capacities of upper extremity. Ergonomics 55, 69–77.
Jacquier-Bret, J., Rezzoug, N., Gorce, P., 2013. Effect of spinal cord injury at C6–C7 on global upper-limb coordination during grasping: manipulability approach. IRBM 34, 69–73.
Klein, C.A., Blaho, B.E., 1987. Dexterity measures for the design and control of kinematically redundant manipulators. Int. J. Robot. Res. 6, 72–83.
Kobayashi, Y., Minami, M., Yanou, A., Maeba, T., 2013. Dynamic reconfiguration manipulability analyses of humanoid bipedal walking. IEEE, Karlsruhe, Germany, pp. 4779–4784.
Minami, M., Zhang, T., Yu, F., Nakamura, Y., Yasukura, O., Song, W., Yanou, A., Deng, M., 2010. Reconfiguration manipulability analyses for redundant robots in view of strucuture and shape, SCIS & ISIS SCIS & ISIS 2010. Jpn. Soc. Fuzzy Theory Intell. Inform., 971–976
Potocanac, Z., de Bruin, J., van der Veen, S., Verschueren, S., van Dieën, J., Duysens, J., Pijnappels, M., 2014. Fast online corrections of tripping responses. Exp. Brain Res. 232, 3579–3590.
Potocanac, Z., Pijnappels, M., Verschueren, S., van Dieën, J., Duysens, J., 2016. Two-stage muscle activity responses in decisions about leg movement adjustments during trip recovery. J. Neurophysiol. 115, 143–156.
Pratt, J.E., Tedrake, R., 2006. Velocity-based stability margins for fast bipedal walking. In: Fast Motions in Biomechanics and Robotics. Springer, pp. 299–324.
Roos, P., McGuigan, P., Trewartha, G., 2009. Trip recovery strategy selection in younger and older adults and the associated physical demands. 33rd Annual American Society of Biomechanics (ASB) Meeting, State College, PA, USA.
Spong, M.W., Hutchinson, S., Vidyasagar, M., 2006. Robot Modeling and Control. John Wiley & Sons, New York.
Vahrenkamp, N., Asfour, T., Metta, G., Sandini, G., Dillmann, R., 2012. Manipulability analysis. IEEE, Osaka, Japan, pp. 568–573.
Wang, T.Y., Bhatt, T., Yang, F., Pai, Y.C., 2012. Adaptive control reduces trip-induced forward gait instability among young adults. J. Biomech. 45, 1169–1175.
Winter, D.A., 2009. Biomechanics and Motor Control of Human Movement. John Wiley & Sons, New York.
Xiang, Y., Arora, J.S., Abdel-Malek, K., 2010. Physics-based modeling and simulation of human walking: a review of optimization-based and other approaches. Struct. Multidiscip. Optim. 42, 1–23.
Yoshikawa, T., 1985a. Dynamic manipulability of robot manipulators. IEEE, pp. 1033–1038.
Yoshikawa, T., 1985b. Manipulability of robotic mechanisms. Int. J. Robot. Res. 4, 3–9.
Yoshikawa, T., 1990. Foundations of Robotics: Analysis and Control. MIT Press, Cambridge, MA.
Zhao, X., Huang, Q., Peng, Z., Li, K., 2004. Kinematics mapping and similarity evaluation of humanoid motion based on human motion capture. 2004 IEEE/RSJ International Conference on Intelligent Robots and Systems, 2004. (IROS 2004) Sendai, Japan, pp. 840–845.